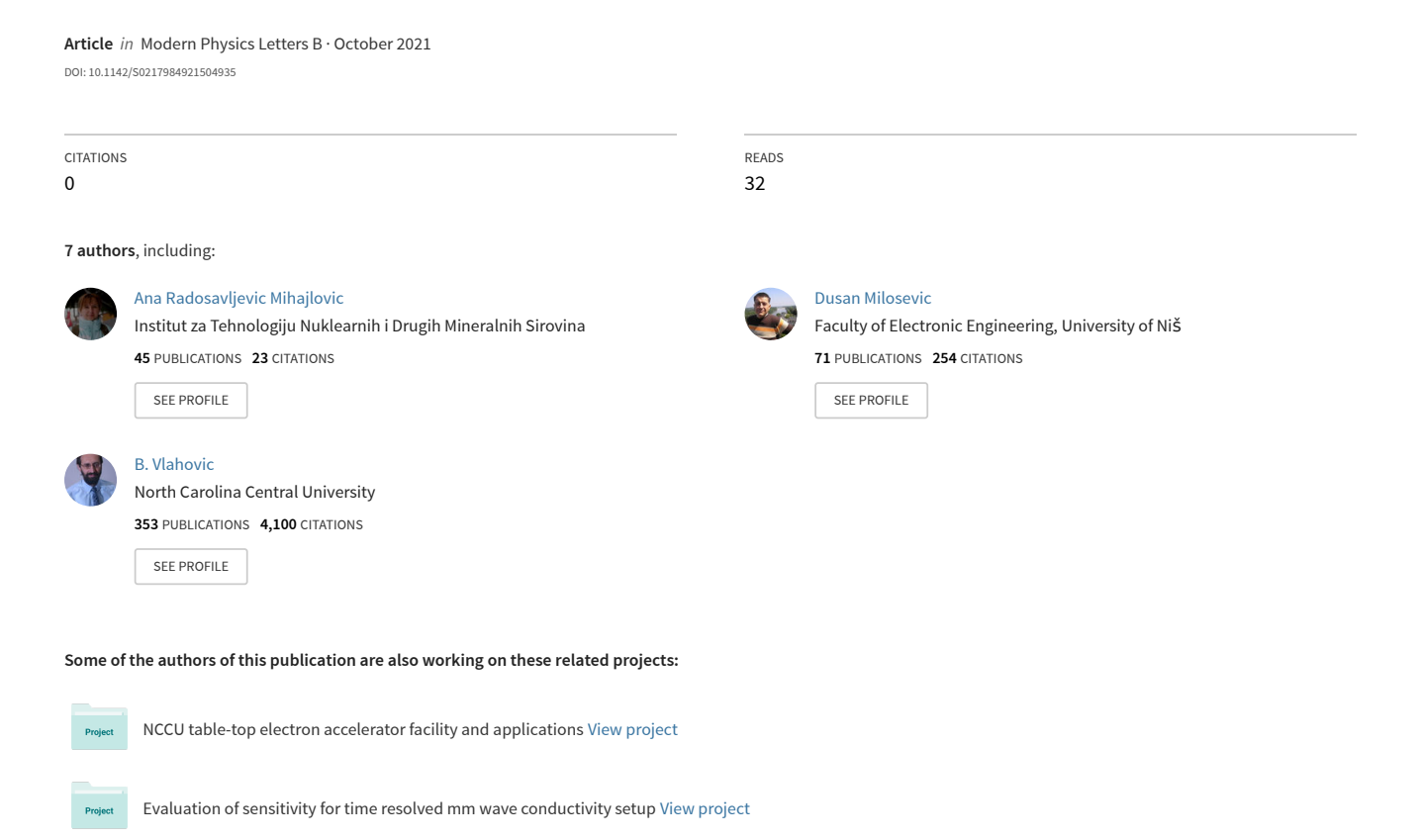
Forensic science and fractal nature analysis





Forensic science and fractal nature analysis

Vojislav V. Mitić*, f, Goran Lazović^{‡, ||}, Ana S. Radosavljevic-Mihajlovic^{§,**},

Dusan Milosević*, †† and Bojana Marković*, †‡

*Faculty of Electronic Engineering, University of Nis,

14 Aleksandra Medvedeva, Nis 18000, Serbia

†Institute of Technical Sciences of SASA, 35 Kneza Mihaila,

Belgrade 11000, Serbia

‡Faculty of Mechanical Engineering, University of Belgrade,

16 Kraljice Marije, Belgrade 11000, Serbia

§Institute for Technology Nuclear and Other Raw Materials,

86 Franse d'Epere Blvd., Belgrade 11000, Serbia

¶vmitic.d2480@gmail.com

|| glazovic@mas.bg.ac.rs

**a.radosavljevic@itnms.ac.rs

††dusan.milosevic@elfak.ni.ac.rs

‡†bojana.markovic123@gmail.com

Dragan Simeunović

Academy of National Security Republic of Serbia, Kraljice Ana, Belgrade 11000, Serbia dragan.simeun@amail.com

Branislav Vlahović

North Carolina Central University, 1801 Fayetteville Street, Durham, NC 27707, USA vlahovic@nccu.edu

> Received 27 June 2021 Revised 4 August 2021 Accepted 17 August 2021 Published 7 October 2021

Forensic photography, also referred to as crime scene photography, is an activity that records the initial appearance of the crime scene and physical evidence in order to provide a permanent record for the court. Nowadays, we cannot imagine a crime scene investigation without photographic evidence. Crime or accident scene photographs can often be reanalyzed in cold cases or when the images need to be enlarged to show critical details. Fractals are rough or fragmented geometric shapes that can be subdivided into parts, each of which is a reduced copy of the whole. Fractal dimension (FD) is an important fractal geometry feature. There are many applications of fractals in various forensic fields, including image processing, image analysis, texture segmentation, shape classification, and identifying the image features such as roughness and smoothness of an

[¶]Corresponding author.

image. Fractal analysis is applicable in forensic archeology and paleontology, as well. The damaged image can be reviewed, analyzed, and reconstructed by fractal nature analysis.

Keywords: Forensic photography; forensic engineering; cultural heritage and historic photographs analysis; crime scene investigation; digital analysis and biometrics analysis; fractals

1. Introduction

From the aspect of forensic science, it is very important to characterize properties of the collected material, like shape, morphology, or microstructure, in order to examine and further investigate the evidence. If there are some blurred or missing parts presented in forensic photography, they can be reconstructed by fractal analysis. Thus, one of the numerous applications of fractal nature analysis^{1,2} is in forensic science. Forensic photography (Fig. 1), also referred to as the crime scene photography,³ improved by fractal analysis, can be implemented in various fields, like criminology, paleontology (Fig. 2), archeology, cultural and historical heritage studies, biometrics, etc.

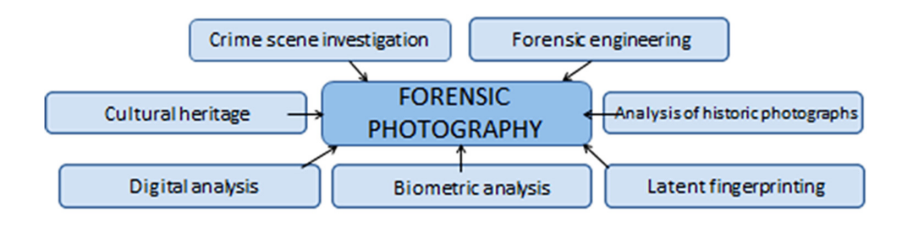


Fig. 1. (Color online) Applications of forensic photography.



Fig. 2. (Color online) Possible objects for fractal analysis application in forensics (a) Jericho⁵; (b) Petra⁶; (c) Pompeii⁷; (d) trilobite fossil⁸; (e) mammoth teeth⁹; (f) plant fossils.¹⁰

Political and religious extremists, during numerous wars, destroyed a number of precious, thousands of years old archeological monuments, demolished religious objects, burned down numerous archives of priceless historical value.⁴ The fractal analysis plays a significant role in the reconstruction of damaged historical artifacts.

Different archeological objects, buildings, or even whole cities, destroyed by natural catastrophes like Pompeii by Vesuvius eruption, or by terrorists like the ancient city of Petra, can be successfully reconstructed applying fractal nature analysis (Fig. 2). Natural clay is one of the first constructing materials used, thus, the fractal clay samples characterization could be very helpful for reconstructing even the oldest human civilization settlements, like the city of Jericho which was all built of clay ceramic material.

In the early 20th century, it became clear that Euclidean geometry is not sufficient to describe some seemingly common phenomena such as chaotic motion, turbulence, crystal growth, and so on. There have appeared some partial solutions, but in the 80s of the 20th century, these attempts were systematized by Mandelbrot in his epochal book, 11 which cast a new light on the order of things in nature. The term fractal is a neologism derived from the Latin adjective fractus meaning fragmented, irregular. Due to its complexity, ¹² a fractal object cannot be successfully defined without involving infinity. In Ref. 11, many examples of fractal phenomena in nature are given: they are all amorphous or hyper-complex structures such as the clouds formation, swirling water, ocean currents motion, polarized light, stars arrangement in galaxies, vegetation, relief irregular forms, the coastline contours, lung tissue alveolar configuration, and many more. In addition to the morphological sphere, fractals appear in the functional sphere, too. For example, noise in telecommunications, free-market price fluctuations, the biomass variation of different plant and animal species, or the statistical performance of spoken language all have a fractal structure.

Fractals are geometric objects having broken, fragmented, wrinkled, or amorphous forms or being highly irregular in some other way. ¹³ Euclidean geometry fails to describe such objects so that they are subjects of fractal geometry.

The topological dimension (TD) describes the common, intuitive dimension of Euclidean geometry objects, with TD = 1 for curves, 2 for surfaces, 3 for solids, etc. The natural extension of the TD that recognizes fractals is the fractal (Hausdorff) dimension (FD). Unlike the TD, FD is typically a noninteger for a fractal object. For example, a calm liquid surface has TD = FD = 2, i.e. the superficial layer of liquid molecules can be approximated as a mathematical plane. Any disturbance, for example by heating, will make the surface geometry more complicated, with $2 < \mathrm{FD} \le 3$. The upper limit, FD = 3 can occur through evaporation of all liquid particles, transforming the planar layer into a three-dimensional (3D) space.

It may be noted that FD is not a unique descriptor. It is likely that fractal structures or patterns can have the same FD but be dramatically different. There are many other fractal descriptors.

1.1. Fractals and self-similarity

Fractals are objects that possess strict geometric self-similarity, they are invariant upon similarity transformation (homothety), like Cantor triadic set, Koch curve, Sierpinski triangle, Menger sponge, etc. (Fig. 3).

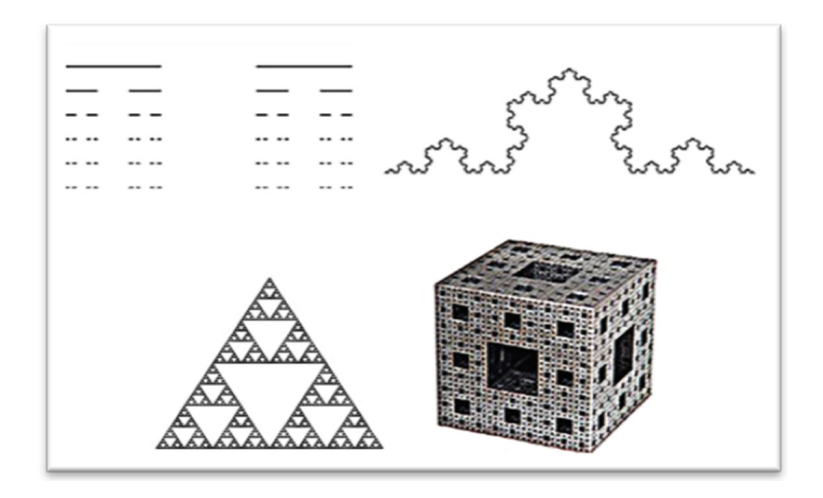


Fig. 3. Classical fractals.

The self-similar object is composed of N copies of itself (with possible translations and rotations), each of which is scaled down by the ratio r in all E coordinates from the whole. More formally, consider a set S of points

$$\mathbf{x} = (x_1, x_2, \dots, x_E) \tag{1}$$

in Euclidean space of dimension E. Under a similarity transform with real scaling ratio 0 < r < 1, the set S becomes rS with points:

$$r\mathbf{x} = (rx_1, rx_2, \dots, rx_E). \tag{2}$$

A bounded set S is self-similar when S is the union of N distinct (non-overlapping) subsets each of which is congruent to rS. Congruent means identical under translations and rotations. The fractal or similarity dimension FD of bounded set S is then given by

$$1 = Nr^{\text{FD}},\tag{3}$$

i.e.

$$FD = \frac{\log N}{\log \frac{1}{r}}.$$
 (4)

This relation leads to several important methods of estimating FD for a given bounded set S.

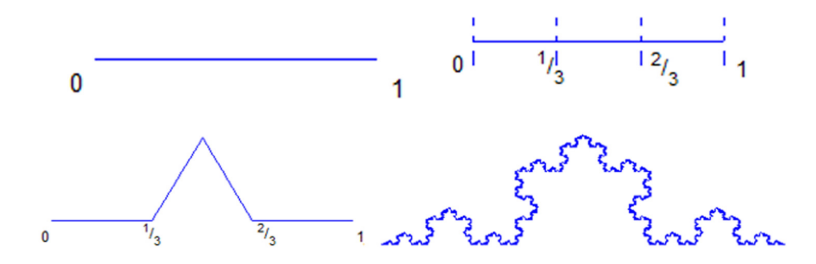


Fig. 4. (Color online) Koch curve.

The typical way to generate fractals is with recursion. Because fractals are comprised of self-similar versions of themselves at smaller scales (which in turn are, themselves, comprised of smaller versions of themselves, etc.), we can start with our desired dimension and recurse down until the required depth (precision) is achieved.

To generate a Koch curve, we start with a unit length line segment. Next, divide this line segment into three equal segments. Then remove the middle section and replace it with two sides of an equilateral triangle with sides that are the same length as the removed segment. This procedure is repeated on each of four segments arbitrarily many times (Fig. 4).

Obviously, N = 4, r = 1/3 so, Koch curve FD is

$$D = \log 4 / \log 3 = 1.26. \tag{5}$$

1.1.1. Fractional Brownian motion and statistical self-similarity

Unlike mentioned ideal (mathematical) fractals, real (physical) fractals are approximately close to their ideal counterparts, they are called pre-fractals (or proto-fractals) and typical examples include trees, forests, Earth relief, microparticles, pores labyrinth in porous materials, etc. Real fractals are made up of parts that resemble the whole in some other way. Sometimes, the resemblance may be only approximate or statistical.

The set S is statistically self-similar if it is composed of N distinct subsets each of which is scaled down by the ratio r from the original and is identical in all statistical respects to rS. A real-valued stochastic process $(X(t): t \ge 0)$ is self-similar if for any r > 0, there exists s > 0 such that

$$X(rt) = sX(t), (6)$$

or equivalently if there exists a unique H>0 (Hurst parameter) such that for any r>0 we have

$$X(rt) = r^H X(t). (7)$$

A mean-zero Gaussian process $(B_H(t): t \ge 0)$ is a fractional Brownian motion with

Hurst parameter H if

$$E[B_H(t)B_H(s)] = \frac{1}{2}(t^{2H} + s^{2H} - |t - s|^{2H})E[B_H^2(1)].$$
(8)

For H = 1/2, we get standard Brownian motion:

$$E[B_H(t)B_H(s)] = \frac{1}{2}(t+s-|t-s|)E[B_H^2(1)]$$

$$= \min(t,s)E[B_H^2(1)]. \tag{9}$$

Some properties of fractional Brownian motion B_H are as follows:

- Stationary increments: Process $Y(t) = B_H(t+s) B_H(s)$; $t \ge 0$ has the same distribution as B_H . Thus, the incremental behavior of B_H at any point in the future is the same.
- Self-similarity: Process $Z(t) = B_H(at); t \ge 0$ has the same distribution as $a^H B_H$. It means the scale invariance of the process: in each time interval the behavior is the same.
- Dependence of increments:
 - \circ For $H \in (0, 1/2)$, the BH has the property of counter persistence: if it was increasing in the past, it is more likely to decrease in the future, and vice versa.
 - \circ For $H \in (1/2, 1)$, the B_H is persistent, it is more likely to keep trend than to break it.
 - \circ For H=1/2 (Brownian motion) has independent increments.
- Fractional Brownian motion is continuous process.

From (3), it follows that

$$E[(B_H(t) - B_H(s))^2] = |t - s|^{2H} E[B_H^2(1)].$$
(10)

So, variance of increment $B_H(t) - B_H(s)$ is proportional to $|t - s|^{2H}$.

It can be shown that FD of fractional Brownian motion trajectory is 11,24,26

$$FD = 2 - H. \tag{11}$$

1.1.2. 1D Fractal interpolation

Suppose that the line segment over which the fractal curve y = y(x) is to be interpolated is [a, b] and let its length be $\delta = b - a$. The values y = y(x) are known on endpoints a, b of the given line segment [a, b] and let the FD of curve y = y(x)be FD = 2 - H.

Values y = y(x) could be considered as a random variable realizations whose increments are normally distributed with mean 0 and variance proportional to $|x_2$ $x_1|^{2H}, x_1, x_2\epsilon [a, b].$

$$y(x_2) - y(x_1) : N(0, |x_2 - x_1|^{2H} \sigma^2).$$
 (12)

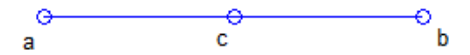


Fig. 5. (Color online) Line segment midpoint interpolation.

First step is to interpolate y = y(x) at midpoint c = (a+b)/2 of given line segment [a, b] (Fig. 5).

It is natural to assume that the values at the ends a, b of line segment [a, b] influence the value at c and that this influence is proportional to their distance from c. Since c is the midpoint, influences are equal

$$y(c) = \frac{y(a) + y(b)}{2} + D_1, \tag{13}$$

where D_1 is a Gaussian random variable with mean 0 and variance Δ_1^2 . This is the so-called random midpoint displacement algorithm.¹⁴ Rewriting the above relation gives

$$y(c) - y(a) = \frac{y(b) - y(a)}{2} + D_1.$$
(14)

Obviously,

$$d(a,c) = d(b,c) = \frac{\delta}{2},$$

$$d(a,b) = \delta.$$
 (15)

Taking variance, we get

$$\left(\frac{\delta}{2}\right)^{2H}\sigma^2 = \frac{1}{4}\delta^{2H}\sigma^2 + \Delta_1^2,\tag{16}$$

$$\Delta_n^2 = (1 - 2^{2H-2}) \left(\frac{\delta}{2^n}\right)^{2H} \sigma^2.$$
 (17)

Note that $\Delta_n^2 \stackrel{H \to 1}{\longrightarrow} 0$.

1.1.3. 1D Fractal extrapolation

Obviously, in a similar way, like in the fractal interpolation, the fractal curve, y = y(x), could be extrapolated. Let b be the midpoint of line segment [a, c] (the same way it could be considered a midpoint of line segment [c, b]).

It holds

$$y(b) = \frac{y(a) + y(c)}{2} + D_1. \tag{18}$$

Since

$$d(a,b) = d(b,c) = \delta,$$

$$d(a,c) = 2\delta,$$
 (19)

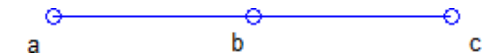


Fig. 6. (Color online) Line segment midpoint extrapolation.

with $\lambda = 2\delta$, we get the same way as in the case of interpolation, the variance of random variable D_1

$$\Delta_1^2 = (1 - 2^{2H-2}) \left(\frac{\lambda}{2}\right)^{2H} \sigma^2, \tag{20}$$

i.e.

$$y(c) = 2y(b) - y(a) - D_1, (21)$$

where $Z_1 = -D_1$: $N(0, \Delta_1^2)$

$$\Delta_1^2 = (1 - 2^{2H-2})\delta^{2H}\sigma^2. \tag{22}$$

Further, this procedure could be recursively continued on line segment [b, c]. By combining interpolation and extrapolation fractal curve could be approximated on the arbitrary line segment.

Extrapolation is quite similar to interpolation. The slight difference is in the matter that interval from interpolation we propose as the interval for extrapolation. In that way, we build the extrapolated structure for the right point (in the case from Fig. 6) based always on the previous calculated point at the beginning of the extrapolation interval. This fact is basically important or rebuilding missing parts within forensic applications, as part of finger points, stamp (as a result from criminal actions), archeological (defected parts under the volcanic ash after magma processes like Vesuvius case on the city of Pompeii or similar), and paleontological (defected samples from different part layers, which are affected of different climate catastrophe).

1.1.4. Statistical self-similarity in n-dimensional space

The formalism of a self-similar fractional Brownian motion $B_H(t)$ in 1D can be easily extended to provide a self-similar fractional Brownian function, $B_H(x)$, $\mathbf{x} = (x_1, x_2, \dots, x_n)$ in *n*-dimensional Euclidean space.

Then, B_H satisfies the general scaling relation

$$E[(B_H(\mathbf{u}) - B_H(\mathbf{v}))^2] \sim |\mathbf{u} - \mathbf{v}|^{2H}$$
(23)

and has an FD

$$FD = n + 1 - H. \tag{24}$$

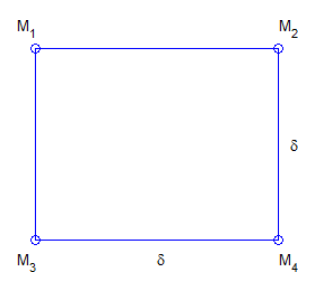


Fig. 7. (Color online) Interpolation area.

1.1.5. 2D Fractal interpolation

Suppose that area over which the fractal surface z = z(x, y) is to be interpolated lies in the square $M_1M_3M_4M_2$ with sides of length δ (Fig. 7) surrounding area D. The values z = z(x, y) are known on vertices M_1 , M_2 , M_3 , and M_4 of the given square and let FD of surface z be FD = 3 – H.

Surface z=z(x,y) could be considered as random variable whose increments are normally distributed with mean 0 and variance proportional to $||(x_2-x_1,y_2-y_1)||^{2H}$, (x_1,y_1) , $(x_2,y_2)\epsilon D$.

$$z(x_2, y_2) - z(x_1, y_1) : N(0, ||(x_2 - x_1, y_2 - y_1)||^{2H} \sigma^2).$$
 (25)

First step is to interpolate z=z(x,y) at midpoint M_c of given square (Fig. 8). Generally, as interpolated value, it can be used as a weighted average of values at the given number of the closest points, ¹⁵ that is, variation of classical midpoint displacement. ¹⁴ Weight could represent individual influence on value to be interpolated so, it could be assumed that weight is inversely proportional to a distance.

In the case of the square midpoint, distances M_1M_c , M_2M_c , M_3M_c , M_4M_c are equal, so weights are equal

$$z(M_c) = \frac{z(M_1) + z(M_2) + z(M_3) + z(M_4)}{4} + D_1, \tag{26}$$

where D_1 is random Gaussian variable with mean 0 and variance Δ_1^2 . Rewriting

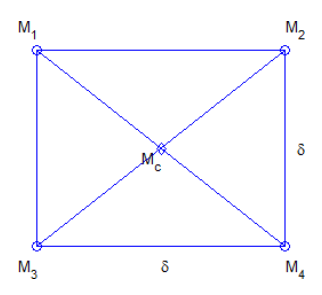


Fig. 8. (Color online) Square midpoint interpolation.

the above relation gives

$$\frac{z(M_c) - z(M_3)}{2} + \frac{z(M_c) - z(M_4)}{2} \\
= \frac{z(M_1) - z(M_4)}{4} + \frac{z(M_2) - z(M_3)}{4} + D_1.$$
(27)

Obviously

$$d(M_c, M_3) = d(M_c, M_4) = \frac{\delta}{\sqrt{2}},$$
 (28)

$$d(M_1, M_4) = d(M_2, M_3) = \sqrt{2\delta}.$$
(29)

Taking variance, we get

$$2\frac{1}{4} \left(\frac{\delta}{\sqrt{2}}\right)^{2H} \sigma^2 = 2\frac{1}{16} (\sqrt{2}\delta)^{2H} \sigma^2 + \Delta_1^2$$
 (30)

and corresponding variance is

$$\Delta_1^2 = \left(\frac{1}{2} - \frac{1}{8}2^{2H}\right) \left(\frac{\delta}{\sqrt{2}}\right)^{2H} \sigma^2$$

$$= \frac{\delta^{2H}}{2^{H+1}} \sigma^2 (1 - 2^{2H-2}). \tag{31}$$

Note that $\Delta_1^2 \xrightarrow{H \to 1} 0$.

Next, extrapolate/interpolate values of z=z(x,y) are at square sides midpoints M_{ij} (Fig. 9).

In the case of midpoint M_{12} , we have

$$d(M_{12}, M_c) = \frac{\delta}{2},\tag{32}$$

$$d(M_1, M_c) = d(M_2, M_c) = \frac{\delta}{\sqrt{2}},$$
(33)

so, weighted average of values at M_1 , M_2 , M_c is

$$z(M_{12}) = \frac{w_1 z(M_1) + w_2 z(M_2) + w_c z(M_c)}{w_1 + w_2 + w_c} + D_2,$$
(34)

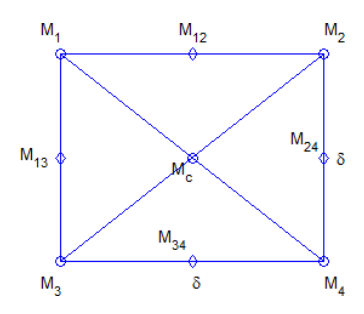


Fig. 9. (Color online) Second step, square sides midpoints interpolation.

where D_2 is Gaussian random variable with mean 0 and variance Δ_2^2 , and weights w_1, w_2, w_c could be

$$w_1 = w_2 = \left(\frac{2}{\delta}\right)^p,\tag{35}$$

$$w_c = \left(\frac{\sqrt{2}}{\delta}\right)^p \tag{36}$$

for some power p > 0.

According to this, from relation (10), we obtain

$$z(M_{12}) = \frac{\left(\frac{2}{\delta}\right)^p z(M_1) + \left(\frac{2}{\delta}\right)^p z(M_2) + \left(\frac{\sqrt{2}}{\delta}\right)^p z(M_c)}{\left(\frac{2}{\delta}\right)^p + \left(\frac{2}{\delta}\right)^p + \left(\frac{\sqrt{2}}{\delta}\right)^p} + D_2(p)$$

$$= \frac{\sqrt{2}^p z(M_1) + \sqrt{2}^p z(M_2) + z(M_c)}{2\sqrt{2}^p + 1} + D_2(p). \tag{37}$$

Rewriting the above relation gives

$$z(M_{12}) - z(M_c) = \frac{\sqrt{2}^p(z(M_1) - z(M_c)) + \sqrt{2}^p(z(M_2) - z(M_c))}{2\sqrt{2}^p + 1} + D_2(p).$$
 (38)

Taking variance, we get

$$\left(\frac{\delta}{2}\right)^{2H} \sigma^2 = 2 \frac{2^p}{(2\sqrt{2}^p + 1)^2} \left(\frac{\delta}{\sqrt{2}}\right)^{2H} \sigma^2 + \Delta_2^2(p), \tag{39}$$

$$\Delta_2^2(p) = \frac{\delta^{2H}}{2^{2H}} \sigma^2 \left(1 - \frac{2^{p+1}}{(2\sqrt{2}^p + 1)^2} 2^H \right). \tag{40}$$

Note that

$$\Delta_2^2(\infty) \sim \frac{\delta^{2H}}{2^{2H}} \sigma^2 (1 - 2^{H-1}) \stackrel{H \to 1}{\longrightarrow} 0. \tag{41}$$

This procedure could be recursively continued on each of four squares $M_1M_{13}M_cM_{12}$, $M_{12}M_cM_{24}M_2$, $M_{13}M_3M_{34}M_c$, $M_cM_{34}M_4M_{24}$ (Fig. 10), with sides of length $\delta/2$.

Forensic science is still quite a new research area still permanently developing. From this point of view, the process of introducing important novelty with fractal nature analysis and methods is very important. From these points of view, we try to explain all of these steps in advanced procedure completely consequently to avoid any misunderstanding and to provide clear direction for readers and researchers in forensic sciences, archeology, paleontology, and criminology as well. In that sense, all mathematical steps are developed step by step and resulting in one from previous and maybe for someone who is in material science research looks as mathematics to much complex, but it is necessary because we for the first time contribute fractal nature analysis in forensics as quite a new solution which opens many frontiers.

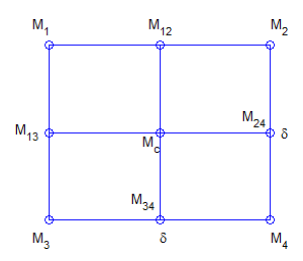


Fig. 10. (Color online) Recursive procedure continuation.

2. Experimental Part

2.1. Ceramic clay consolidation and characterization

The natural clay from the western deposit in Serbia was used for the fractal analysis experiment. The ceramic clay deposits, situated in Mio–Pliocene sediments of the western part of the Tamnava Tertiary Basin (Western Serbia), was discovered in the middle of the last century. Most parts of these deposits are located in the areas of the villages Donje and Gornje Crniljevo with active open pits of gray—white clays Bele Vode and Zbegovi. The production of gray—white ceramic clay is about 100,000 tons per annum, and the total reserves are estimated at over 50 million tons. ¹⁶

Raw ceramic clay composites had high SiO_2 contents, moderate Al_2O_3 contents, and low contents of other oxides. The Fe_2O_3 contents varied; in the gray—white and dark composite clays, they were below 2 wt.%. EPMA of sample 3 (lamellar clay) was performed on red and white—yellow lamellae.

The grain size values were generally unique, and according to the distribution, the ceramic clays from the active deposits belong to poor sandy-powder clays.

The X-ray powder and crystallographic analysis 17 of the natural sample of clay (can constitute any material as long as it is within the particle size range of $< 2~\mu m$) are presented in Fig. 11. According to the X-ray diffraction pattern (Fig. 11), the mineralogical composition was as follows: kaolinite, illite/hydromica, mica, quartz, and feldspar. 18

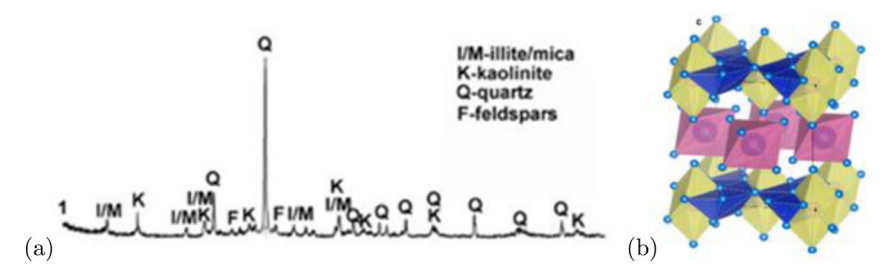


Fig. 11. (Color online) (a) The X-ray powder diffraction pattern of natural clay from deposit Tamnava; (b) the crystal structure of natural clay from deposit Tamnava.

2.2. Preparation for the fractal analysis

We prepared several samples at different magnifications within the diapason from 500 to 10,000 times. We selected just one sample for the analysis and prepared one scanning microscope image of mineral kaolinite at the magnification of 6000 times for the fractal analysis (Fig. 12).

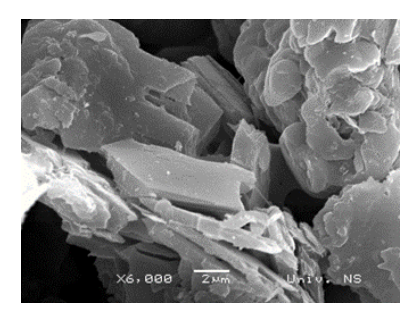


Fig. 12. SEM image of kaolinite prepared for fractal analysis.

In this research, we used four SEM images of the same part of the sample at four different magnifications for the fractal analysis (Fig. 13).

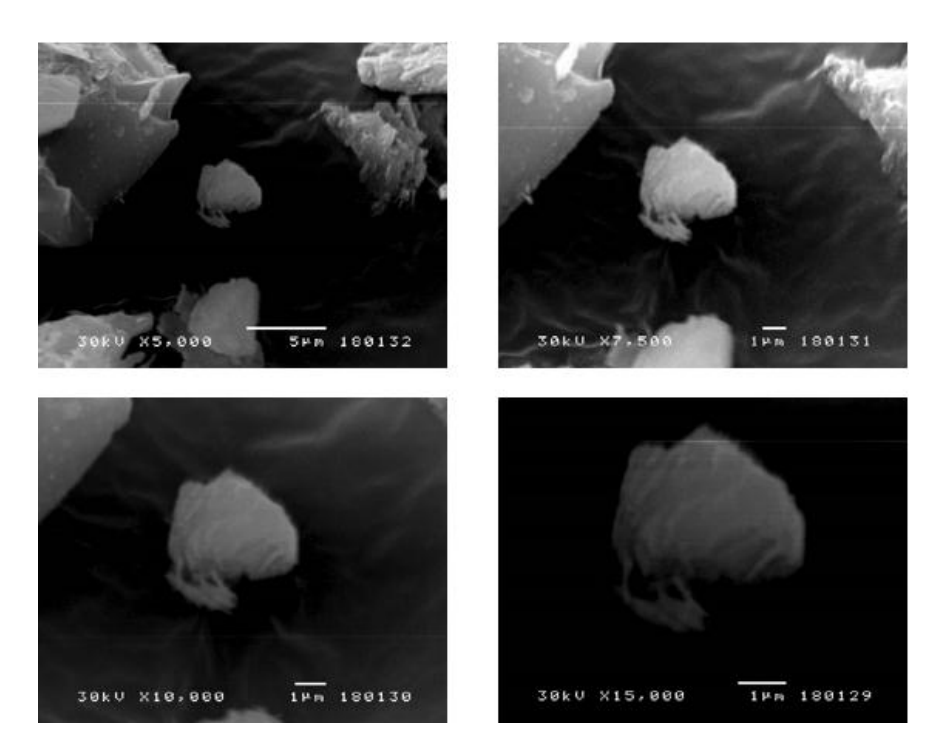


Fig. 13. SEM images of the same part of the sample at four different magnifications.

3. Results and Discussion

In this research paper, the natural clay examination results are presented. This natural ceramic material is chosen because the majority of archeological artifacts are related to clay items or object fragments. It should be emphasized that clay had been used as a construction material for safeguarding walls, settlements, and cottages since ancient times. Various analytical methods are used for clay artifacts archeological research, ¹⁹ and we introduce fractal characterization as an additional technique. Let us consider that the fractal analysis was applied on prepared SEM images of clay samples.

By applying fractal characterization²⁰ and fractal reconstruction, we can determine and predict²¹ microstructure, morphology, and shape²² of ceramic clay samples, important for further forensic analysis. The FD is the essential characteristic of every fractal object, as it defines its morphological and microstructural properties. One of the most exploited methods for estimating the FD is the box-counting (BC) method, where N, plotted on the y-axis as $\log(N)$, presents the number of boxes covering the fractal pattern and h, plotted on the x-axis as $\log(h)$, presents the magnification. Based on the obtained graph, we can calculate FD represented by the slope of the line, which is calculated by applying the least-squares method. To estimate FD, the central linear part of the line is to be considered. A higher

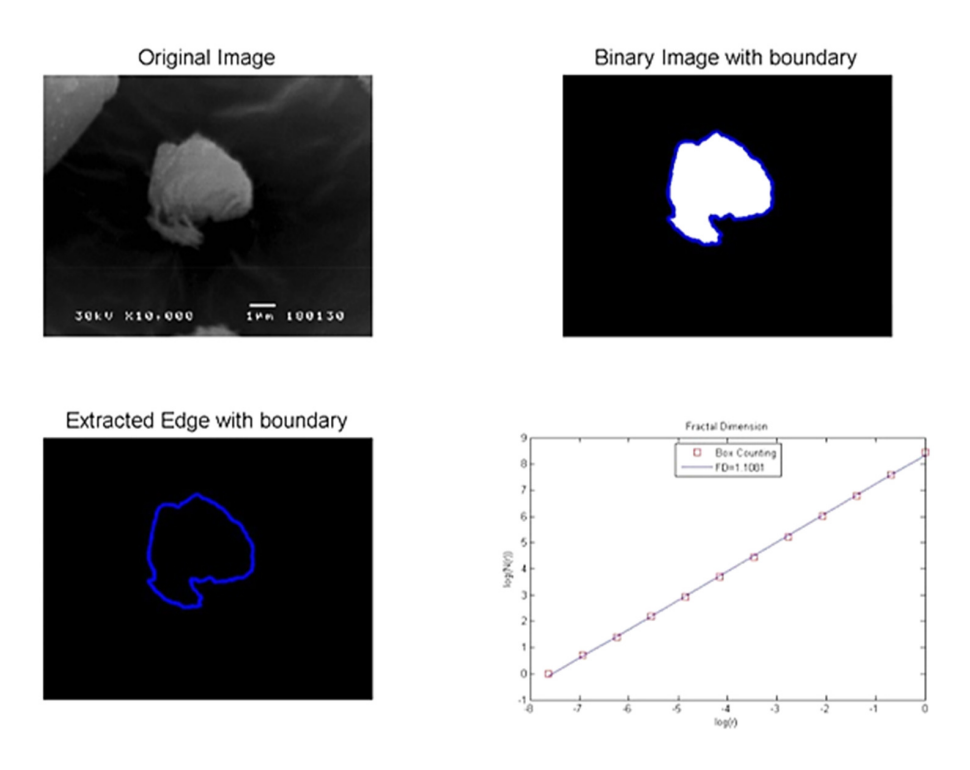


Fig. 14. (Color online) Fractalization of the sample.

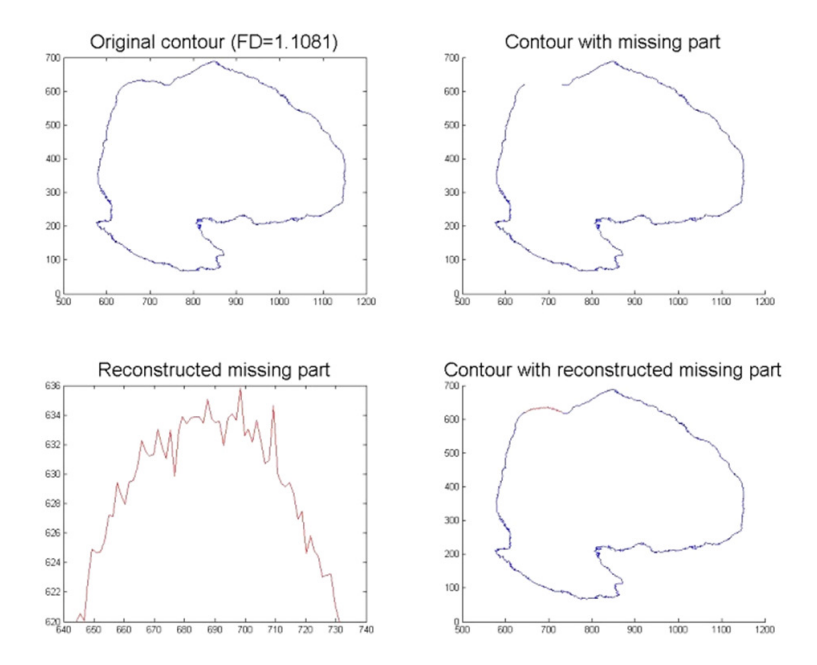


Fig. 15. (Color online) Reconstructing pathway of the contour's missing part by fractal analysis.

slope designates increasing object complexity with the decreasing box size, while a lower slope designates that the details do not appear as fast as magnification grows i.e. the object is of a more linear shape.

Thus, by implementing the BC method, we can obtain FD, which precisely determines the ceramic clay sample's shape and microstructure.²¹ Therefore, we applied the BC method on the original SEM image, and in a few steps shown in Fig. 14, we obtained FDs for the given sample. The estimated FD, which is used for shape characterization, is FD = 1.1081.

Based on previous research and results, by applying fractal nature analysis, we successfully developed a method for microstructure morphology shapes reconstruction. In all of these fractals, self-similarity and biomimetic approaches from the real nature are reached and completed the whole concept in applied fractalization. The main idea, that we can reconstruct some morphology shapes by fractal analysis, opens the frontiers for predicting and designing microstructure shapes or morphology, what is leading toward predicting and projecting morphological shapes or just parts of them. So, the variety of sample sources are from archeology, paleontology, and also in different areas of criminology. Regarding all of these mentioned, we open the doors for extended forensic samples and problems solutions and applications.

In forensic science, there is often evidence (presented on the forensic photographs) which are damaged or has missing parts, thus, their reconstruction to the original state is necessary. To reconstruct the original shape and microstructure fractal analysis can be applied^{23,24} (Fig. 15). In the sense of better clarification of

the reconstruction methodology, we expressed the statement that once when we can collect the points of the reconstructed object, we can also predict the points, the morphology of the structures within we can recognize the complete shape of some part at the image of the sample and on that way to cover missed data.

All these results and original novelties in fractal applications open the door for future extended research with some specific characteristics directed separately to different areas of archeology, paleontology, and specific forensic in criminology.

4. Outlook

In our future research, we plan to continue developing the "fractal forensic" on different examples within an extension of cases, shapes, morphological shapes, and samples. In that direction, we plan to apply examples to illustrate how to perform the complicated mathematical equations to real cases in addition to the existing ones.

5. Conclusion

The main idea of this paper is related to a very important issue that comes up from different sources like archeology, paleontology, or also criminology. The major problem to be overcome is how to reconstruct the morphological shapes that miss some parts, and our goal is to provide the solution.

Numerous archeological artifacts are destroyed over a long time period or due to some catastrophes, like earthquakes or volcanic eruptions. For example, that could be ceramic pottery from Vinca, Egyptian sculptures, Roman weapons, Greek columns, or medieval fortress debris, and our idea is to reconstruct these historical samples to get better insight into the ancient civilizations' epoch. The analysis of clay tablets with imprinted writings and their reconstruction represents a very important segment in ancient written documents defining.

Introducing the fractal approach is significant for paleontological science, as well. Fossil remains like bones or teeth imprints of various animals could be reconstructed applying fractal analysis. It could be a valuable source providing information about some huge animals, like mammoths which disappeared during the ice age. Floral fossils can also be characterized by this method.

When it comes to common criminal and terrorism, as well, forensic evidence fractal analysis²⁵ is of great importance. The main developing idea is that we can use some forensic tracks from criminal cases where we have just partial fingerprints, which we can reconstruct to obtain the missing parts. This is one significant original approach for acquiring the complete primary trace from the partial one.

Based on the forensic clues improved by fractal analysis, we come to very interesting and important conclusions. This research paper aimed to introduce the ceramic clay samples fractal characterization to the forensic field, and regarding that, we successfully reconstructed the missing part of the contour applying fractal analysis. Considering the vast forensic field, our future research will be directed toward implementing fractal reconstruction on various significant forensic subjects.

Now, we can stress that this method could be applied to different samples materials because all conclusive samples could be based on different materials extended on different materials. The application of fractal analysis in forensic science opens new frontiers for more accurate and more precise examination of archeological, pale-ontological, and criminological material sources leading to their deeper and better understanding, which have an important impact on our present.

References

- V. V. Mitić, G. Lazović, D. Mirjanic, H. Fecht, B. Vlahović and W. Arnold, Mod. Phys. Lett. B 34 (2020) 2050421.
- V. V. Mitić, P.-Y. Chen, Y.-Y. Chou, I. D. Ilic, B. Marković and G. Lazović, Mod. Phys. Lett. B 35 (2021) 2150318.
- 3. M. T. Miller and P. Massey, *The Crime Scene: A Visual Guide* (Academic Press, San Diego, 2015), p. 45.
- 4. D. Simeunović, 4th Serbian Ceramic Society Conf. ACA IV (2015), p. 38.
- A. Valavanidis and T. Vlachogianni, Sci. Adv. Environ. Toxicol. Ecotoxicol. 4 (2013)
- G. Delmonaco, C. Margottini and D. Spizzichino, Rock fall hazard assessment in the Siq of Petra, Jordan, in *Landslide Science and Practice: Risk Assessment, Manage*ment and Mitigation, eds. P. Canuti, C. Margottini and K. Sassa, Vol. 6 (Springer, Heidelberg, 2013), p. 441.
- F. Garzia, F. Borghini, A. Bruni, M. Lombardi, P. Mighetto, S. Ramalingam and S. B. Russo, Int. J. Saf. Secur. Eng. 10 (2020) 11.
- 8. W. Itano, Trilobite Tales 37 (2019) 17.
- 9. A. M. Lister, V. Dimitrijević, Z. Marković, S. Knezević and D. Mol, Quat. Int. (2012).
- S. G. Lucas, W. A. DiMichele and B. D. Allen, New Mexico Mus. Nat. Hist. Sci. Bull. 84 (2021).
- 11. B. B. Mandelbrot, The Fractal Geometry of Nature (W. H. Freeman, New York, 1977).
- V. V. Mitić, G. Lazović, V. Paunović, J. R. Hwu, S.-C. Tsay, T.-P. Perng, S. Veljković and B. Vlahović, J. Eur. Ceram. Soc. 39 (2019) 3513.
- O. Zmeškal, M. Veselý, M. Nežádal and M. Buchniček, HarFA Harmonic Fractal Image Analysis (2001), pp. 3–5.
- M. F. Barnsley, R. L. Devaney, B. B. Mandelbrot, H.-O. Peitgen, D. Saupe and R. F. Voss, The Science of Fractal Images (Springer Verlag, New York, 1988).
- D. F. Watson, Contouring: A Guide to the Analysis and Display of Spatial Data (Pergamon Press, Oxford, 1992).
- S. Radosavljević, J. Stojanović, A. Radosavljevic-Mihajlovic, N. Vuković, S. Matijasević and M. Stojanović, Ann. Geol. Penins. Balk. 75 (2014) 75.
- A. S. Radosavljevic-Mihajlovic, A. S. Daković, V. D. Kasic, V. V. Mitić, J. N. Stojanović, M. D. Sokić and B. R. Marković, Hem. Ind. 72 (2018) 371.
- S. Radosavljević, R. Milicević and B. Panic, in Proc. 11th Congr. Geologist of Yugoslavia (1986), p. 357.
- M. N. Stanković, N. S. Krstić, D. M. Đorđević, N. Anastasijević, V. V. Mitić, G. A. Topličić-Ćurčić and A. J. Momčilović-Petronijević, Sci. Sinter. 51 (2019) 233.
- 20. V. V. Mitić, G. Lazović, J. Ž. Manojlović, W.-C. Huang, M. M. Stojiljković, H. Facht and B. Vlahović, *Therm. Sci.* **24** (2020) 2203.

V. V. Mitić et al.

- V. V. Mitić, G. Lazović, V. Paunović, N. Cvetković, D. Jovanović, S. Veljković,
 B. Randjelović and B. Vlahović, Ceram. Int. 45 (2019) 20475.
- V. V. Mitić, G. Lazović, V. Paunović, S. Veljković, B. Randjelović, B. Vlahović and H. Fecht, Ferroelectrics 545 (2019) 184.
- V. V. Mitić, H.-J. Fecht, M. Mohr, G. Lazović and L. Kocić, AIP Adv. 8 (2018) 075024.
- V. V. Mitić, L. Kocić, V. Paunović, G. Lazović and M. Miljković, *Mater. Res. Bull.* 101 (2018) 175, https://doi.org/10.1016/j.materresbull.2018.01.019.
- 25. D. J. S. Barrera, Q. H. S. Relatorres and K. R. Rosento, UV J. Res. 7 (2013) 35.
- V. V. Mitić, L. Kocić, V. Paunović, F. Bastić and D. Sirmić, Sci. Sinter. 47(2) (2015) 195.